JCTC Journal of Chemical Theory and Computation

Article

pubs.acs.org/JCTC

When Density Functional Approximations Meet Iron Oxides

Yu Meng,[†,‡,§] Xing-Wu Liu,[†,‡,§] Chun-Fang Huo,[‡] Wen-Ping Guo,[‡] Dong-Bo Cao,[†,‡] Qing Peng,[∥] Albert Dearden,[⊥] Xavier Gonze,[#] Yong Yang,[†,‡] Jianguo Wang,[†] Haijun Jiao,[†,▽] Yongwang Li,*[,†,‡] and Xiao-Dong Wen*[,†,‡]

[†]State Key Laboratory of Coal Conversion, Institute of Coal Chemistry, Chinese Academy of Sciences, Taiyuan 030001, P. R. China

[‡]National Energy Center for Coal to Clean Fuels, Synfuels China Co., Ltd., Huairou District, Beijing 101400, P. R. China

[§]University of Chinese Academy of Sciences, No. 19A Yuquan Road, Beijing 100049, P. R. China

[∥]Department of Mechanical, Aerospace and Nuclear Engineering, Rensselaer Polytechnic Institute, Troy, New York 12180, United States

[⊥]Department of Physics, Berea College, Berea, Kentucky 40403, United States

[#]Institute of Condensed Matter and Nanosciences, Université Catholique de Louvain, Louvain-la-Neuve, Belgium

[▽]Leibniz-Institut für Katalyse e.V., Universität Rostock, Albert-Einstein Strasse 29a, 18059 Rostock, Germany

Supporting Information

ABSTRACT: Three density functional approximations (DFAs), PBE, PBE+*U*, and Heyd−Scuseria−Ernzerhof screened hybrid functional (HSE), were employed to investigate the geometric, electronic, magnetic, and thermodynamic properties of four iron oxides, namely, α-FeOOH, α-Fe_2O_3, Fe_3O_4, and FeO. Comparing our calculated results with available experimental data, we found that HSE (a = 0.15) (containing 15% "screened" Hartree−Fock exchange) can provide reliable values of lattice constants, Fe magnetic moments, band gaps, and formation energies of all four iron oxides, while standard HSE (a = 0.25) seriously overestimates the band gaps and formation energies. For PBE+*U*, a suitable *U* value can give quite good results for the electronic properties of each iron oxide, but it is challenging to accurately get other properties of the four iron oxides using the same *U* value. Subsequently, we calculated the Gibbs free energies of transformation reactions among iron oxides using the HSE (a = 0.15) functional and plotted the equilibrium phase diagrams of the iron oxide system under various conditions, which provide reliable theoretical insight into the phase transformations of iron oxides.

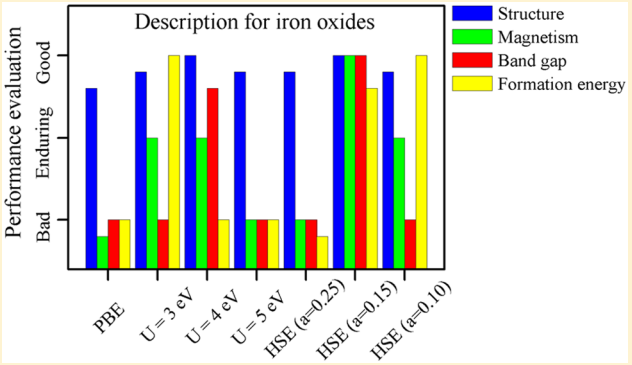

1. INTRODUCTION

Iron oxides have been the focus of numerous studies because of their great application potential in many disciplines,[1−6] such as geology, mineralogy, biology, medicine, physics, and various kinds of chemistry. These polymorphs have diverse structures and readily undergo phase transformations among themselves. In particular, α-FeOOH, α-Fe_2O_3, Fe_3O_4, and FeO are the most common compositions in many heterogeneous catalysts.[7−9] For instance, iron oxides are vital components in Fischer−Tropsch synthesis, which converts syngas (CO and H_2) to clean liquid fuels and highly valuable chemicals.[6,10,11]

It has been a challenge[12−14] to accurately describe the electronic and magnetic properties, especially the electronic band gap, of iron oxides by conventional density functional theory (DFT) with the local density approximation (LDA) or the generalized gradient approximation (GGA) because of the strongly correlated nature of the d electrons, each of which has a strong influence on its neighbors in iron oxides. For extended systems, the most successfully corrected methods to LDA and GGA are the Hubbard *U* correction (DFT+*U*)[15] and hybrid functionals.[16,17] Extensive studies of the iron oxides (α-FeOOH, α-Fe_2O_3, Fe_3O_4, and FeO) employing various density functional approximations (DFAs), including LDA, GGA, DFT+*U*, and several kinds of hybrid functionals have been reported.[13,18−31] We have summarized their performances with respect to lattice parameters, magnetic moments, and band gaps in Table 1.

Although much work has been focused on iron oxides using different DFAs, from Table 1 it is still difficult to judge which DFA is a good choice for accurately describing both the structure and major properties of iron oxides. There are no predictions of iron oxides at the same DFA level, which are important to link the transformations between different phases. It is well-known that LDA (or GGA) underestimates the band gaps and magnetic moments of iron oxides, which can be improved by the DFT+*U* approach. However, previous studies indicated that each material

Received: June 24, 2016
Published: August 17, 2016

DOI: 10.1021/acs.jctc.6b00640
J. Chem. Theory Comput. 2016, 12, 5132−5144

Table 1. Summary of Previous Work on Structures, Magnetic Moments, and Band Gaps of α-FeOOH, α-Fe_2O_3, Fe_3O_4, and FeO Predicted by Different DFAs

	method	potential/code	lattice constants (Å)	magnetic moment (μ_B)	band gap (eV)	ref(s)
α-FeOOH	LSDA	USPP/CASTEP	a = 9.80 b = 3.00 c = 4.49	–	–	19
	GGA-PBE	USPP/CASTEP	a = 9.87 b = 3.006 c = 4.66	3.74	0.8	37
	PBE+U (5.2 eV)		a = 10.15 b = 3.084 c = 4.646	4.16	2.5	
	GGA-PBE	PAW/VASP	a = 9.94 b = 2.99 c = 4.60	–	–	18
	PBE+U (3 eV)		a = 9.95 b = 3.00 c = 4.60	–	–	
	PBE+U (4 eV)	FP-LAPW+lo/wien2k	–	4.13	2.21	38
	GGA-PW91	PAW/VASP	a = 9.978 b = 3.002 c = 4.631	3.54	0.77	20
	PW91+U (3 eV)		a = 10.03 b = 3.033 c = 4.630	4.10	1.97	
	HSE06		a = 9.964 b = 3.011 c = 4.569	4.18	3.80	
	expt		a = 9.81 b = 2.97 c = 4.53	3.82	2.1	1, 39
α-Fe_2O_3	GGA-PW91	VASP	a = 4.997 c = 13.854	3.44	0.3	24
	PW91+U (5–9 eV)		–	4.6	2.0	
	B3LYP	basis set/crystal	a = 5.12 c = 13.82	4.16	3.0	26
	LDA	PAW/VASP	–	–	0.0	21, 30
	GGA-PBE		a = 5.070 c = 13.816	3.6	0.5	
	LDA+U (4.3 eV)		a = 4.982 c = 13.576	4.1	2.0	
	PBE+U (4.3 eV)		a = 5.104 c = 13.907	4.2	2.0	
	HSE06		a = 5.046 c = 13.750	4.1	3.5	
	PBE0		a = 5.047 c = 13.753	4.1	4.2	
	PBE	PAW/VASP	–	3.60	0.67	25
	PBE0		–	4.60	15.58	
	HSE06		–	4.16	3.41	
	HSE(12%)		–	4.16	1.95	
	expt		a = 5.04 c = 13.75	4.6–4.7	2.0–2.2	40–43
LT-Fe_3O_4	LSD	muffin-tin-orbital/ASA	–	A:3.46–3.48 B:3.39–3.57	0	44
	LSD+SIC		–	A:4.00–4.08 B:3.83–3.97	0.35	
	LDA+U (3.6 eV)	PAW/VASP	–	B:3.39–3.90	0.2	28
	LDA+U (4 eV)	PAW/VASP	–	B:3.48–3.94	0.18	29
	B3LYP	basis set/crystal	–	A:4.15 B:3.73–4.26	0.87	22
	expt		a = 5.94	3.59–3.76	0.14	45–47

DOI: 10.1021/acs.jctc.6b00640
J. Chem. Theory Comput. 2016, 12, 5132–5144

Table 1. continued

	method	potential/code	lattice constants (Å)	magnetic moment (μ_B)	band gap (eV)	ref(s)
			b = 5.92 c = 16.78			
FeO	GGA-PBE	PAW/VASP	4.268	3.59	–	
	PBE+U (5 eV)		4.333	3.74	–	31
	LDA+U (3.7 eV)	PAW/VASP	–	–	1.6	30
	LDA	FP-LAPW+lo/wien2k	4.18	3.44	0.0	13
	PBE		4.3	3.49	0.0	
	LDA+U (5.91 eV)		4.28	4.23	2.20	
	B3PW91		4.35	4.15	1.80	
	PBE0		4.40	4.30	1.60	
	B3LYP	basis set/crystal	4.365	–	3.70	23
	HF		4.311	–	14.05	
	GGA		–	3.40	0.0	
	GGA+U (3 eV)	PAW/VASP	–	3.60	–	48
	HSE03		–	3.60	2.2	
	expt		4.33	3.32–4.2	0.5, 2.4	49–51

generally needs a semiempirical U value for an accurate description of its electronic properties. The Heyd–Scuseria–Ernzerhof screened hybrid functional (HSE)[32,33] incorporating a fraction of Hartree–Fock (HF) exchange into the short-range exchange interaction has been proposed and successfully applied to strong correlation systems.[34−36] Although to some extent HSE would also require a material-dependent amount of HF exchange, it should be emphasized that the optimized choice of one unique parameter entering the HSE hybrid functional was found to precisely reproduce the magnetic and electronic properties of a wide class of systems.[17] The summary also indicates that there has not yet been a consistent DFA that can be used to accurately reproduce the structures and major properties of a group of iron oxides (α-FeOOH, α-Fe_2O_3, Fe_3O_4, and FeO). However, in order to make meaningful quantitative property comparisons of the iron oxides by DFT, it is crucial to choose a proper and consistent DFA to calculate the properties of iron oxides. Despite the extensive studies, there is still the need for a systematic evaluation of the performances of DFAs capable of correctly predicting the most properties for all iron oxides on the ground-state properties of the above-mentioned iron oxides.

In this work, we present a systematic investigation of the ground-state properties, including structural, electronic, and magnetic properties and formation energies, of α-FeOOH, α-Fe_2O_3, Fe_3O_4, and FeO using the Perdew–Burke–Ernzerhof (PBE), PBE+U, and HSE approximations. Furthermore, we predict the Gibbs free energies of the phase transformations among given iron oxides and plot the thermodynamic equilibrium phase diagrams of these four iron oxides under oxidizing and reducing atmospheres. The current study provides theoretical insights into tracing down the phase diagram of iron oxides during reaction from a reliable and consistent DFA, which is of significance to tune the phase composition by changing the external conditions.

2. THEORETICAL METHODS AND COMPUTATIONAL DETAILS

2.1. PBE, PBE+U_{eff}, and HSE Calculations. All of the calculations were carried out using the projector-augmented wave (PAW)[52] pseudopotential with a plane-wave cutoff energy of 400 eV as implemented in the Vienna Ab Initio Simulation Package (VASP).[53] Three types of exchange–correlation (xc) functionals were applied: (1) the standard PBE functional;[54] (2) the PBE+U method utilizing the scheme of Dudarev[55] with several effective U values (U_{eff} = 1, 2, 3, 4, 5, and 6 eV); (3) the HSE screened hybrid functional.[32]

As shown in eq 1, the exchange energy (E_x^{HSC}) is separated into short-range (SR) and long-range (LR) components in the HSE functional. The SR part includes both HF ($E_x^{HF,SR}$) and PBE ($E_x^{PBE,SR}$) terms, and the LR part has only a PBE term ($E_x^{PBE,LR}$). Here a is the HF exchange mixing coefficient and ω is a splitting parameter that defines the partitioning between the SR and LR components, which was adjusted to reproduce PBE hybrid heats of formation in molecules with some consideration given to band gaps in materials.[33]

$$E_{xc}^{HSE} = aE_x^{HF,SR}(\omega) + (1 - a)E_x^{PBE,SR}(\omega) + E_x^{PBE,LR}(\omega) + E_c^{PBE} \quad (1)$$

In this work, ω was defined as 0.2 $Å^{-1}$ as originally suggested by Heyd et al.,[32] which typically gives good-quality results for many cases.[33] As derived from perturbation theory,[17] the value of the parameter a in the HSE functional was 0.25, which can accurately predict enthalpies of formation, ionization potentials, and electron affinities for molecules as well as lattice constants and band gaps for solids.[36,56] However, as reported, standard HSE with a = 0.25 overestimates the band gaps of α-FeOOH and α-Fe_2O_3.[20,57] It is recognized that the optimal amount of HF exchange is actually system-dependent.[33] In this work, to get good results for iron oxides, the HSE functionals with a = 0.15 and a = 0.10, denoted as HSE (a = 0.15) and HSE (a = 0.10), respectively, were also tested, considering that the more HF exchange leads to the prediction of bigger band gaps of semiconductors and insulators.[13]

All of the crystal structures were optimized without any constraints on volume, shape, or internal structural parameters. The convergence criteria for the electronic self-consistent iterations and forces were set to 10^{-5} eV and 0.02 eV/ Å, respectively. The Γ-point-centered Monkhorst–Pack (MP) k mesh scheme was used in all of the calculations. For PBE and PBE+U calculations, we used (7 × 3 × 10), (4 × 4 × 4), (7 × 7 × 2), and (11 × 11 × 11) k meshes for α-FeOOH, α-Fe_2O_3, Fe_3O_4, and FeO, respectively. For HSE calculations, the k meshes for α-FeOOH, α-Fe_2O_3, Fe_3O_4, and FeO were reduced to (3 × 2 × 5), (4 × 4 × 4), (3 × 3 × 1), and (6 × 6 × 6), respectively, to reduce the computational cost. We checked the convergence of the small

DOI: 10.1021/acs.jctc.6b00640
J. Chem. Theory Comput. 2016, 12, 5132−5144

Table 2. Some Basic Properties of α-FeOOH, α-Fe_2O_3, Fe_3O_4, and FeO[1]

	color	Fe valence	Fe site	O packing	space group symbol and number	magnetic ordering
α-FeOOH	yellow-brown	+3	oct.	hcp	$P\frac{21}{n}\frac{21}{m}\frac{21}{a}$	AFM
α-Fe_2O_3	red	+3	oct.	hcp	$P\bar{3}\frac{2}{c}$	AFM
Fe_3O_4	black	+2, +3	oct., tet.	fcc	$P1\frac{2}{c}1$	FiM
FeO	black	+2	oct.	fcc	$F\frac{4}{m}\bar{3}\frac{2}{m}$	AFM

Table 3. Lattice Constants (Å) of the Four Iron Oxides Calculated Using the PBE, PBE+U (4 eV), HSE (a = 0.25), and HSE (a = 0.15) Approaches; The Corresponding Experimental Values and the MAEs (in Å) and MAREs (in %) over the Lattice Parameters Are Also Presented

				HSE		
		PBE	U = 4 eV	a = 0.25	a = 0.15	expt
α-FeOOH	a	4.57	4.56	4.54	4.54	4.53[a]
	b	9.88	9.93	9.88	9.88	9.81[a]
	c	2.98	3.01	3.00	2.99	2.97[a]
	MAE	0.04	0.07	0.04	0.04	–
	MARE	0.6	1.1	0.6	0.6	–
α-Fe_2O_3	$a = b$	5.05	5.04	5.00	5.00	5.04[b]
	c	13.68	13.73	13.62	13.67	13.75[b]
	MAE	0.06	0.01	0.06	0.05	–
	MARE	0.4	0.2	0.7	0.5	–
Fe_3O_4	a	5.94	5.97	5.97	5.93	5.94[c]
	b	5.93	5.96	5.96	5.89	5.92[c]
	c	16.69	16.79	16.79	16.67	16.78[c]
	MAE	0.02	0.03	0.03	0.05	–
	MARE	0.2	0.4	0.4	0.5	–
FeO	$a = b = c$	4.30	4.34	4.32	4.30	4.33[d]
	MAE	0.03	0.01	0.01	0.03	–
	MARE	0.6	0.3	0.2	0.8	–

[a]Reference 1. [b]Reference 40. [c]Reference 45. [d]Reference 49.

k meshes by the energy difference between two differently dense k meshes within 50 meV, and the detailed test results are listed in Table S1 in the Supporting Information (SI).

2.2. Thermodynamic Phase Equilibrium Calculations. In the calculation of thermodynamic phase equilibria, the Gibbs free energy (G) of iron oxides can be separated into two contributions, G_{nonmag} and G_{mag}, as shown in eq 2:

$$G = G_{nonmag} + G_{mag} \tag{2}$$

The nonmagnetic Gibbs free energy, G_{nonmag}, includes lattice vibrations (F^{vib}), an electronic contribution (E^{ele}), and a PV term:

$$G_{nonmag} = F_{nonmag} + PV = E^{ele} + F^{vib} + PV \tag{3}$$

In eq 3, E^{ele} is the DFT total energy and F^{vib} is the vibrational contribution including the zero-point energy. For solid iron oxides, the $\Delta(PV)$ term is extremely small and usually ignored.

The magnetic contribution, G_{mag}, was calculated using eq 4:

$$\Delta G_{mag} = \Delta H_m - T\Delta S_m = \int_0^T C_m \, dT + T\int_0^T \frac{C_m}{T} \, dT \tag{4}$$

where the magnetic specific heat (C_m) can be approximated by an empirical equation; a detailed description of the magnetic specific heat is given in Chuang's work.[58]

The reaction entropy is dominated by the entropy of gases, which can be captured by changes in the gas chemical potential, as shown in eq 5:

$$\mu_{gas}(T, P) = E_{gas}^{total} + \tilde{\mu}_{gas}(T, P^0) + k_B T \ln \frac{P_{gas}}{P^0} \tag{5}$$

where E_{gas}^{total} stands for the DFT total energy of the isolated gas-phase molecule (including the zero-point energy) and $\tilde{\mu}_{gas}(T, P^0)$ is the change in chemical potential at different temperatures (including the contributions from vibrations and rotations of the molecule) under standard conditions. In this work, the values of $\tilde{\mu}_{gas}(T, P^0)$ were derived from thermodynamic tables,[66] and the vibrational properties and the zero-point corrections for iron oxides were obtained from lattice phonon calculations using the PHONOPY software.[59] In calculations of phase diagrams, the energy data for magnetite were derived from both the low-temperature monoclinic phase (below 122 K) and the high-temperature cubic phase (above 122 K).

3. RESULTS AND DISCUSSION

3.1. Comparison of Properties Predicted by Different DFAs. Some basic properties of α-FeOOH, α-Fe_2O_3, Fe_3O_4, and FeO are listed in Table 2. The crystal structures of the four iron oxides studied in this work have been derived from experimental measurements, and the detailed lattice parameters are listed in Table 3. Here the structure of magnetite is the low-temperature monoclinic phase.[45] More detailed discussions of the ground-state properties are given in the appropriate subsections. At this point it should be noted that the computations performed structural optimizations simulating the nontrivial magnetic arrangements for α-FeOOH, α-Fe_2O_3, Fe_3O_4, and FeO by

DOI: 10.1021/acs.jctc.6b00640
J. Chem. Theory Comput. 2016, 12, 5132−5144

collinear ferromagnetic (FM), antiferromagnetic (AFM), ferrimagnetic (FiM), and nonmagnetic (NM) orderings of the local magnetic moment. The most stable magnetic orderings predicted by the three DFAs confirmed that α-FeOOH, α-Fe_2O_3, and FeO all have AFM ground states, while Fe_3O_4 is FiM. The detailed results on the relative energies corresponding to the four magnetic orderings using different DFAs are provided in Table S2. In the following, except for the section on magnetic properties, only the results for the most stable magnetic arrangement of each iron oxide will be discussed.

3.1.1. Structural Properties. Structures of iron oxides derived from experimental characterizations were reoptimized using the PBE, PBE+U (4 eV), HSE (a = 0.25), and HSE (a = 0.15) functionals. The calculated lattice parameters together with corresponding experimental data are shown in Table 3. The mean absolute error (MAEs) and the mean absolute relative error (MAREs) over the lattice constants a, b, and c with respect to the experimental data are provided. From the results, one can find that the lattice parameters of α-FeOOH, α-Fe_2O_3, Fe_3O_4, and FeO calculated by PBE, PBE+U (4 eV), HSE (a = 0.25), and HSE (a = 0.15) have very small deviations from the experimental data, with MAEs less than 0.1 Å and MAREs less than 1%. This indicates that PBE can provide a good description of the structures of most iron oxides, while PBE+U and HSE have few improvements in structural description over PBE. In addition, the energy−volume (E−V) curves for the four iron oxides were fit using the third-order Birch−Murnaghan equation of state, as shown in Figure S1 in the SI.

For PBE+U, a detailed analysis of the effect of the value of U on the lattice constants is provided in Figure S2. The U value has small influence on the lattice parameters. We also analyzed the performance of different DFAs on the structures from the relative errors of the volumes (Figure 1 top). The relative errors of the volumes calculated using the three DFAs with respect to the experimental values are all less than 3% for α-FeOOH, α-Fe_2O_3, Fe_3O_4, and FeO. Although PBE provided the volumes with smaller errors than the others, the results from PBE+U and HSE are still good for predicting the volumes of iron oxides. Combined with the results for the lattice parameters, these results lead to the conclusion that one can get good results on the structures of most iron oxides using PBE instead of the complex and time-consuming PBE+U and hybrid functional methods.

3.1.2. Magnetic Properties. The magnetism of iron oxides has been very attractive for a long time because of their particularity. Low-temperature magnetism measurements[1] have shown that α-FeOOH and α-Fe_2O_3 exhibit AFM ordering, Fe_3O_4 displays FiM behavior below the Curie temperature (ca. 850 K), and FeO crystallizes in the AFM-type arrangement below the Neel temperature (ca. 198 K). We performed a series of geometry optimization calculations considering FM, AFM, FiM, and NM magnetic configurations for each oxide within the PBE, PBE+U, and HSE approximations. The calculated most stable magnetic orderings (MOs) for the iron oxides are summarized in Table 4. Besides the most stable magnetic arrangements, the values of the calculated spin magnetic moments (MMs) by different functionals as well as the experimental data for each iron oxide are also provided in Table 4, and the detailed Fe magnetic moments of differently coordinated Fe in Fe_3O_4 are presented in Table S3. From these results, one can find that the four approaches predict a consistent AFM configuration for α-FeOOH and α-Fe_2O_3 and ferrimagnetic order for Fe_3O_4, which agree well with the experimental observations. For FeO, PBE provides a wrong

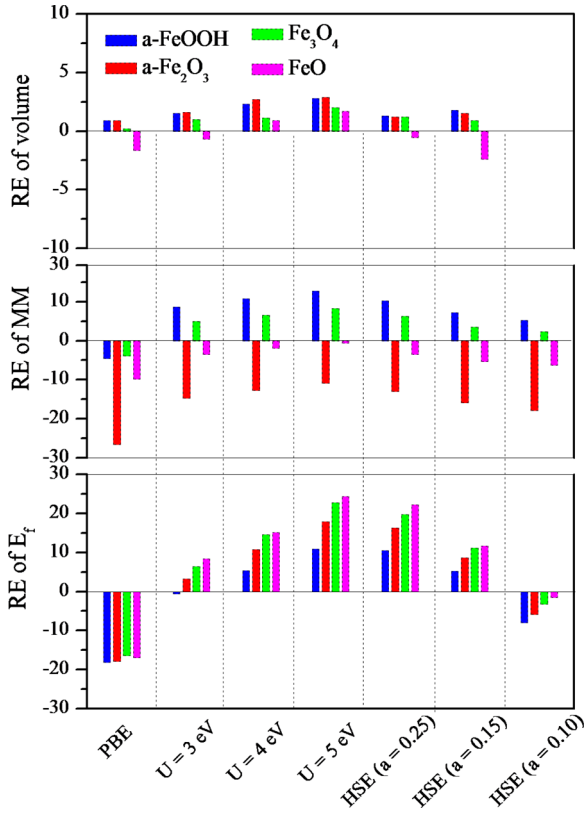

Figure 1. Relative errors of volumes, Fe magnetic moments, and formation energies calculated using different DFAs with respect to the corresponding experimental data.

FM ground state, while PBE+U and HSE give the most stable AFM magnetic ordering, matching experiment well.

In addition, remarkable differences in the spin magnetic moments with different DFAs are observed, and the performance of each functional is not uniform for the four iron oxides (Figure 1 middle). PBE underestimates the magnetic moments of all four iron oxides, especially for FeO and α-Fe_2O_3, with relative errors of 10% and 30%, respectively. PBE+U (U = 3, 4, and 5 eV) and HSE (a = 0.25, 0.15, and 0.10) overestimate the magnetic moments of α-FeOOH and Fe_3O_4 but underestimate those of α-Fe_2O_3 and FeO. For PBE+U, the Fe magnetic moment increases with ascending U_{eff} value for all four iron oxides, and the detailed data about the effect of the U value on the local spin magnetic moment for the four iron oxides are given in Figure S2. For HSE, the Fe magnetic moment decreases as the HF contribution goes down. HSE (a = 0.15) and HSE (a = 0.10) provide relatively acceptable results for α-FeOOH, Fe_3O_4, and FeO. However, all the DFAs underestimate the magnetic moment of α-Fe_2O_3 to different extents.

3.1.3. Band Gaps and Electronic Structures. It is well-established that most iron oxides are semiconductors at low temperature. Apart from the case of α-FeOOH, the electronic properties of other three iron oxides have been extensively investigated using a wide variety of methods. However, a systematic comparison of different DFAs at the same DFT level is still lacking. The band gaps of iron oxides predicted by various DFAs are collected in Table 4. PBE provides α-FeOOH and α-Fe_2O_3 band gaps of 0.3 and 0.44 eV, respectively, which are too much smaller than the experimental values of 2.1−2.5 eV[1] and 2.0 eV.[62] What is worse, Fe_3O_4 and FeO are predicted to be half-metal and metal by PBE, respectively. For the PBE+U method,

DOI: 10.1021/acs.jctc.6b00640
J. Chem. Theory Comput. 2016, 12, 5132−5144

Table 4. Ground-State Magnetic Ordering (MO), Magnetic Moment (MM) (in Units of μ_B per Fe Atom), Band Gap, and Bulk Modulus (BM) for the Four Iron Oxides Calculated Using the PBE, PBE+U (U = 3, 4, and 5 eV), and HSE (a = 0.25, 0.15, and 0.10) Functionals and the Corresponding Experimental Measurements

			U			HSE			
		PBE	3 eV	4 eV	5 eV	0.25	0.15	0.10	expt
α-FeOOH	MO	AFM	–	AFM	–	AFM	AFM	–	AFM
	MM	3.63	4.13	4.21	4.28	4.19	4.08	4.00	3.80(2)[a]
	gap	0.30	1.50	1.80	2.20	3.20	2.00	1.42	2.1[b]
	BM	92.95	–	109.06	–	125.60	120.23	–	111[c]
α-Fe_2O_3	MO	AFM	–	AFM	–	AFM	AFM	–	AFM
	MM	3.49	4.05	4.15	4.23	4.13	4.00	3.90	4.6–4.9[d,e]
	gap	0.44	1.70	2.08	2.42	3.45	2.24	1.66	2.2[f]
	BM	175.17	–	187.56	–	220.50	218.02	–	225[g]
Fe_3O_4	MO	FiM	–	FiM	–	FiM	FiM	–	FiM
	MM	3.53–3.54	3.68–4.04	3.66–4.18	3.7–4.26	3.65–4.17	3.67–3.94	3.65–3.87	3.59–3.76[h]
	gap	0	0	0.48	1.02	0.86	0.12	0.05	0.14[i]
	BM	166.98	–	176.00	–	204.94	185.15	–	183[j]
FeO	MO	FM	–	AFM	–	AFM	AFM	–	AFM
	MM	3.39	3.63	3.69	3.74	3.63	3.56	3.52	3.32–4.2[k,l]
	gap	0	0.36	0.43	0.84	2.32	0.38	0.14	0.5[m]
	BM	180.97	–	166.36	–	179.9	181.31	–	153[n]

[a]Reference 39. [b]Reference 1. [c]Reference 60. [d]Reference 41. [e]Reference 42. [f]Reference 61. [g]Reference 43. [h]Reference 46. [i]Reference 47. [j]Reference 62. [k]Reference 50. [l]Reference 51. [m]Reference 63. [n]Reference 64.

an U_{eff} value of 5, 4, and 3.6 eV give band gaps of 2.2, 2.08, and 0.23 eV for α-FeOOH, α-Fe_2O_3, and Fe_3O_4, respectively, which are in good agreement with experimental measurements. The relationships between the U value and the band gap for the iron oxides are presented in Figure S2. Surprisingly, our results show that HSE (a = 0.25) seriously overestimates the band gaps of iron oxides, despite previous work indicated that the HSE (a = 0.25) functional can accurately predict band gaps of most semiconductors in general.[56] Good prediction of the band gaps of the four iron oxides is achieved using the HSE (a = 0.15) functional. To put the HSE functional in a broader perspective, we also perform calculations with HSE (a = 0.10), which has a greater PBE component, and the results indicate that it significantly underestimates the band gaps of all four iron oxides. To get a direct-viewing impression, in Figure 2 we plot band gaps for the four iron oxides against different DFAs and the experimental data.

The results of Bader charge analysis of the four iron oxides are given in Table S4. PBE provides relatively weak charge transfer between Fe and O, while PBE+U and HSE give enhanced charge transfer. The charges are mainly transferred from Fe 4s and 3d to O 2p, which is closely related to the spin magnetic moment. For instance, the PBE+U and HSE functionals give strong charge transfer from Fe 4s and 3d to O 2p, which is favorable to form more unpaired electrons in the Fe valence orbitals, leading to a larger spin magnetic moment. In addition, one can identify nonequivalence of Fe ions in oxides by charge transfer. For example, PBE shows that the octahedrally coordinated Fe atoms of Fe_3O_4 are equivalent, while PBE+U and HSE functionals indicate that the octahedral Fe are divided into two types with different valences by variant charge transfer. In other words, the PBE+U and HSE methods provide charge ordering of Fe_3O_4 in good agreement with that previously reported.[28,29]

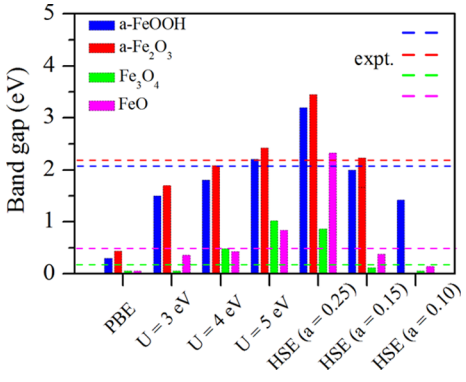

Figure 2. Calculated band gaps for the four iron oxides from the PBE, PBE+U (U = 3, 4, 5 eV), and HSE (a = 0.25, 0.15, 0.10) methods. The corresponding experimental data (expt.) are represented by the dashed lines.

The total density of states (TDOS) and projected density of states (PDOS) of Fe 3d and O 2p for the four iron oxides using PBE, PBE+U, HSE (a = 0.25), and HSE (a = 0.15) are plotted in Figure 3. PBE provides delocalized Fe 3d electrons occupying the energy band from about −10 eV below the Fermi level to the Fermi level in all of the iron oxides, which gives rise to underestimated gaps of α-FeOOH and α-Fe_2O_3 and wrong metal features for Fe_3O_4 and FeO. PBE+U and HSE can correct the drawback of PBE by the introduction of a proper Hubbard U parameter and partial HF exact-exchange energy, respectively. PBE combined with a suitable U value can obtain a reasonable electron distribution with the correct gap type and value for each iron oxide by improving the complex interaction among the d electrons. Detailed investigations of the effect of the U value on the electronic structure for each oxide are presented in Figure S3. For iron oxides, it is found that HSE (a = 0.25) fails to give accurate descriptions of the electronic structures and provides spin polarization interactions for the 3d electrons that are too strong. In contrast, HSE (a = 0.15) provides good results, including the right band-gap types and values, electron distributions, and splitting characteristics of the d electrons by the addition of partial accurate exchange interaction. In order to verify this point, in Figure 4 we compare available experimentally measured X-ray photoemission spectroscopy (PES) and inverse

DOI: 10.1021/acs.jctc.6b00640
J. Chem. Theory Comput. 2016, 12, 5132−5144

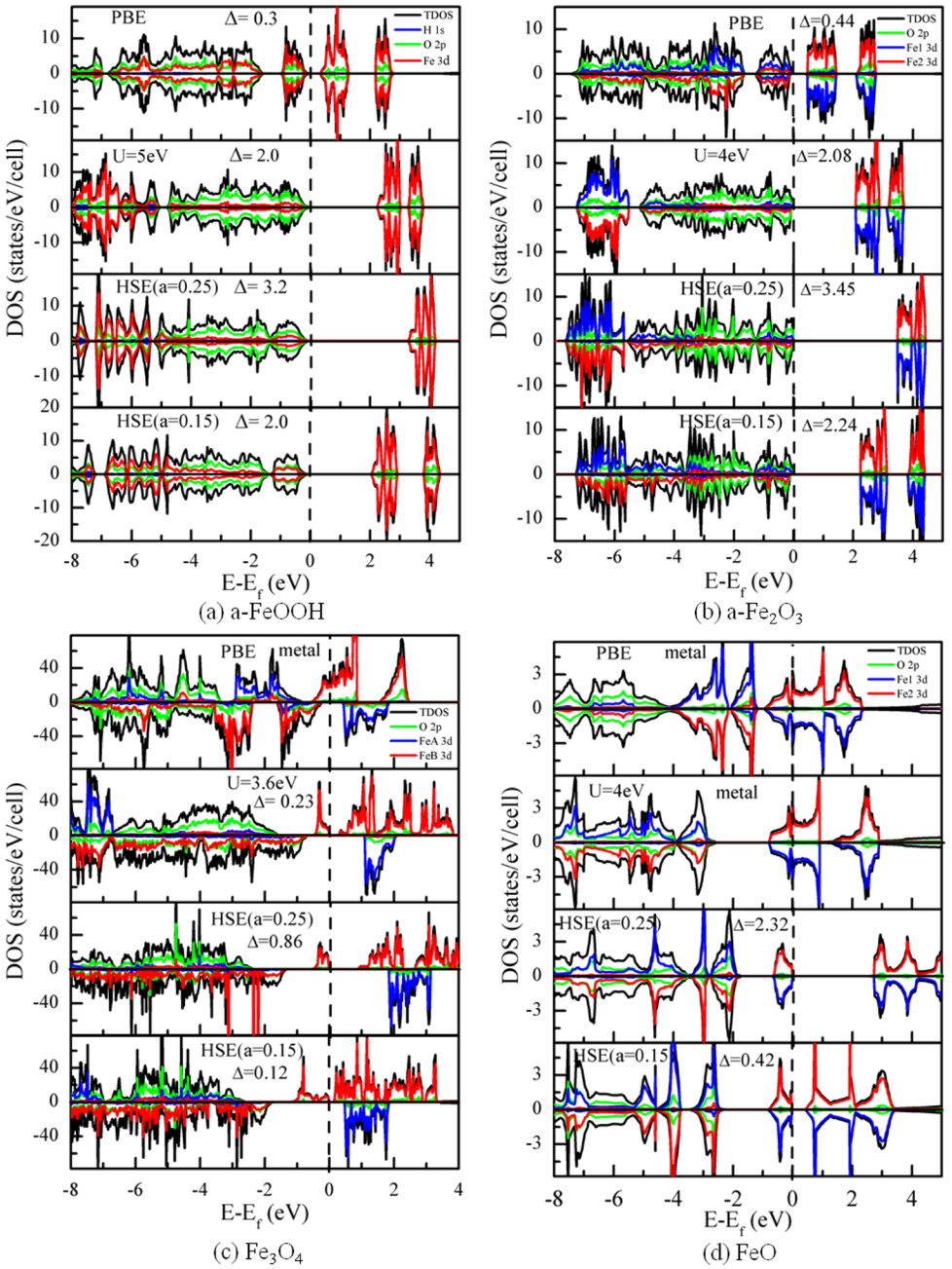

Figure 3. Calculated spin-resolved total density of states (TDOS) and Fe 3d and O 2p densities of states for (a) α-FeOOH, (b) α-Fe_2O_3, (c) Fe_3O_4, and (d) FeO obtained using PBE, PBE+U, HSE (a = 0.25), and HSE (a = 0.15).

photoemission spectroscopy (BIS) data for α-Fe_2O_3 and FeO with our calculated TDOS. It is found that PBE+U (4 eV) and HSE (a = 0.15) predict accurate electron distributions for α-Fe_2O_3 in line with the experimental measurements.[65] For FeO, however, only HSE (a = 0.15) provides electronic features in agreement with the measurements by PES+BIS.[66]

Besides the electronic properties, the dielectric functions predicted by PBE, PBE+U (4 eV), HSE (a = 0.25), and HSE (a = 0.15) for the four iron oxides are presented in Figure S4. For these properties, we cannot say whether the predictions are good or bad since there are no corresponding experimental measurements. To put it another way, a nonbiased, accurate experimental characterization of each pure iron oxide is an important way to calibrate theoretical approaches.

3.1.4. Formation Energies. The energy of formation, ΔH, at T = 0 K is defined as

$$\Delta H = E_{Fe_xO_y} - xE_{Fe} - \frac{y}{2}E_{O_2} \quad (6)$$

in which $E_{Fe_xO_y}$, E_{Fe}, and E_{O_2} are the DFT total energies of the given oxide (subscripts x and y denote the Fe and O compositions, respectively), bulk α-Fe, and O_2, including zero-point vibration corrections, respectively. The calculated formation energies of the iron oxides, available experimental data, and the corresponding MAREs are summarized in Table 5. A clear pictorial view of the relative errors for the iron oxides using different methods is given in the bottom panel of Figure 1 as well. First, the PBE functional shows pronounced underestimation of the formation energies, with a MARE of about 18%.

DOI: 10.1021/acs.jctc.6b00640
J. Chem. Theory Comput. 2016, 12, 5132−5144

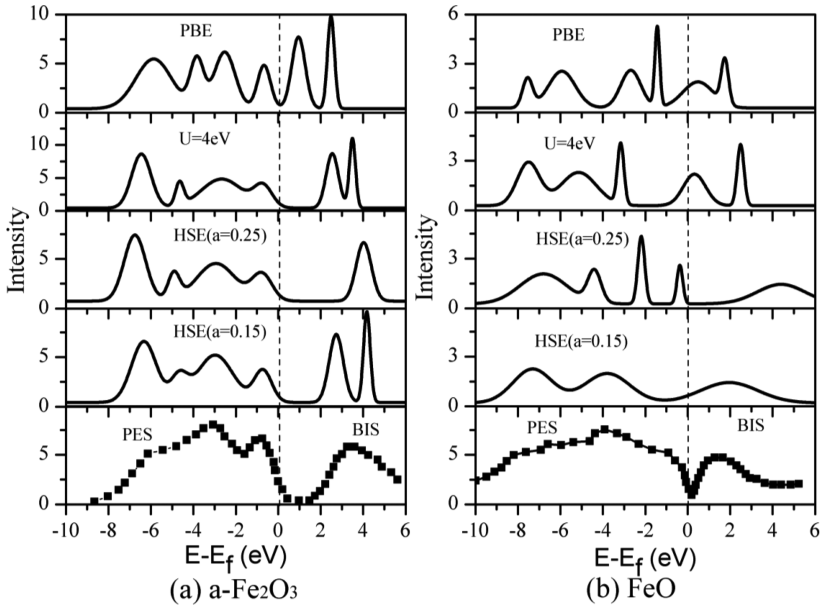

Figure 4. Comparison of measured photoemission (PES) and inverse photoemission (BIS) spectra with theoretical total densities of states obtained using different functionals for (a) α-Fe_2O_3 and (b) FeO.

Table 5. Calculated Formation Energies (in kJ/mol) for the Four Iron Oxides Obtained Using the PBE, PBE+*U* (*U* = 3, 4, 5 eV), and HSE (*a* = 0.25, 0.15, 0.10) Functionals and Their Relative Errors with Respect to the Experimental Data[66]

		α-FeOOH	α-Fe_2O_3	Fe_3O_4	FeO	MARE (%)
PBE		−459.47	−672.68	−931.72	−225.92	17
U	3 eV	−557.57	−845.92	−1185.22	−294.81	5
	4 eV	−590.85	−907.23	−1277.62	−313.13	11
	5 eV	−621.90	−965.05	−1367.68	−338.28	19
HSE	0.25	−619.68	−952.20	−1333.82	−332.43	17
	0.15	−590.13	−890.61	−1238.49	−303.81	9
	0.10	−515.61	−770.77	−1077.96	−267.88	5
expt		−560.70	−819.03	−1114.58	−272.04	

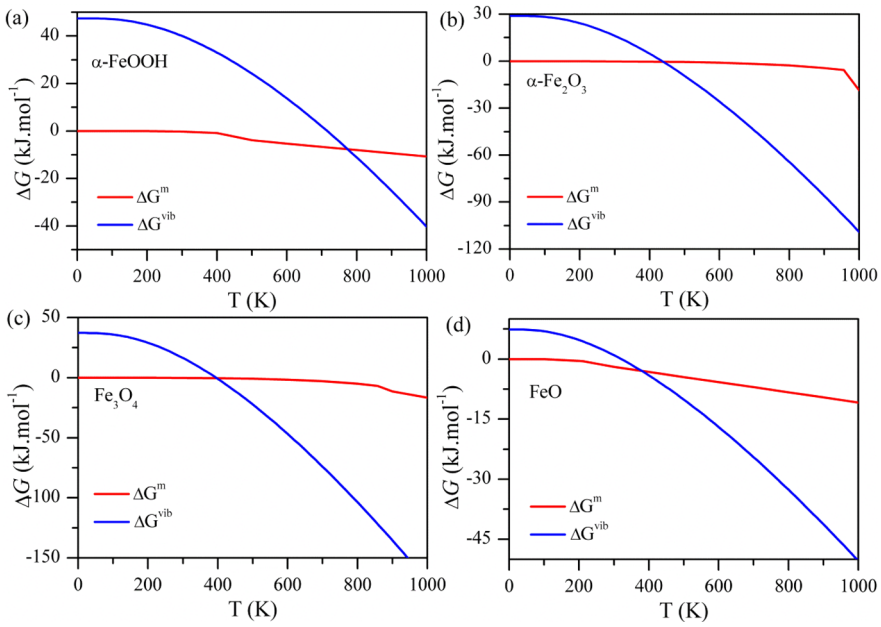

Figure 5. Magnetic (ΔG^m) and phonon (ΔG^{vib}) contributions to the free energies (ΔG).

Markedly improved results are achieved using PBE+*U* combined with a suitable *U* value and the HSE functional with a proper percentage of HF exchange contribution. For PBE+*U*, the formation energies increase with ascending U_{eff} value, and PBE

DOI: 10.1021/acs.jctc.6b00640
J. Chem. Theory Comput. 2016, 12, 5132−5144

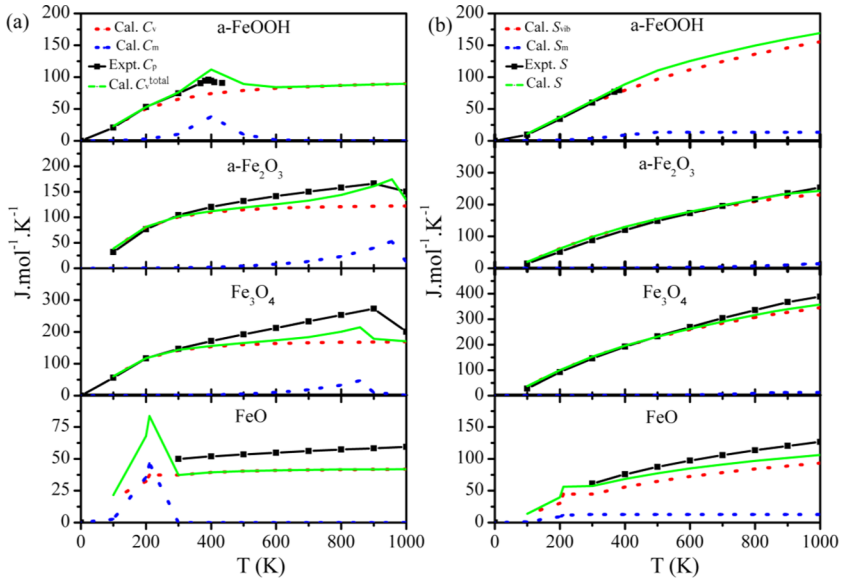

Figure 6. Comparison of the calculated and experimental data for thermodynamic functions of the four iron oxides: (a) calculated total specific heat (Cal. C_v^{total} = Cal. C_v + Cal. C_m), including the calculated lattice (Cal. C_v) and magnetic (Cal. C_m) contributions, and the experimental specific heat (Expt. C_p); (b) calculated entropy (Cal. S = Cal. S_{vib} + Cal. S_m), including calculated vibrational (Cal. S_{vib}) and magnetic (Cal. S_m) contributions, and the experimental entropy (Expt. S).

$+U$ (3 eV) provides good results for the formation energies of the four oxides, with a MARE of about 4%. For the HSE functional, classical HSE (a = 0.25) obviously overestimates the energies of formation of the four iron oxides, with a MARE of 18%. With smaller amounts of HF exchange, HSE (a = 0.15) and HSE (a = 0.10) give the formation energies of iron oxides with MAREs of 9% and 5%, respectively.

3.2. Thermodynamic Phase Diagrams of Iron Oxides. It is known that complicated phase transformations exist in iron oxides under natural and industrial conditions, so understanding the phase equilibria of iron oxides under given conditions is helpful to tune the conditions to obtain the targeted iron oxide. On the basis of the above calculated results, it is found that HSE (a = 0.15) presents reliable results for the structural, magnetic, electronic, and thermodynamic properties of most iron oxides. Hence, we perform thermodynamic calculations on phase transformations among the iron oxides under different atmospheres using the HSE (a = 0.15) functional.

To construct the phase diagrams, we use appropriate free energy models given by eqs 2−5 to calculate the Gibbs free energies of the iron oxides and gases in the system. The vibrational contributions are computed by phonon calculations, and the detailed results are provided in Figure S5. We also take α-Fe_2O_3 as a sample to check the influence of various DFAs on the densities of states of phonons of iron oxides, and the test results are shown in Figure S6. The magnetic and phonon contributions to the free energies are shown in Figure 5. In order to verify the reliability of our calculated magnetic and phonon contribution data, we compare the calculated specific heats and entropies with the experimental specific heats and entropies of the four iron oxides,[66] as shown in Figure 6. One can find that our calculated results reach good agreement with the experimental values to a great extent, and the small deviation may result from the approximation that we neglect the dilation of the lattices (C_p − C_v) for solids and from the differences between the experimental structures and the perfect crystals in this work, considering the inevitable defects in experimental structures.

On basis of the above results, we first investigate the dehydration reaction of α-FeOOH to form α-Fe_2O_3 and H_2O (eq 7):

$$2\mathrm{FeOOH} \rightleftarrows \mathrm{Fe_2O_3} + \mathrm{H_2O}$$
$$\Delta G_r = \Delta G_f(\mathrm{Fe_2O_3}) + \Delta G_f(\mathrm{H_2O}) - 2\Delta G_f(\mathrm{FeOOH}) \quad (7)$$

The reaction Gibbs free energies and equilibrium phase diagram are given in Figure 7a,b. Figure 7a shows that the dehydration is not the thermodynamically spontaneous reaction below the critical temperature (ca. 300 K) at a water pressure of 1 atm. Figure 7b indicates that α-Fe_2O_3 is thermodynamically most stable beyond a critical temperature at a given H_2O pressure, while it becomes unstable when the pressure of H_2O increases to a critical value at a given temperature. Thus, increasing the temperature and reducing the H_2O partial pressure are favorable for dehydration of α-FeOOH to α-Fe_2O_3.

We then also calculate the thermodynamic equilibria for transformations among α-Fe_2O_3, Fe_3O_4, and FeO under O_2 oxidation and H_2 reduction conditions (eqs 8−13):

$$\mathrm{Fe} + \frac{1}{2}\mathrm{O_2} \rightleftarrows \mathrm{FeO}$$
$$\Delta G_r = \Delta G_f(\mathrm{FeO}) - \Delta G_f(\mathrm{Fe}) - \frac{1}{2}\Delta G_f(\mathrm{O_2}) \quad (8)$$

$$\mathrm{FeO} + \frac{1}{6}\mathrm{O_2} \rightleftarrows \frac{1}{3}\mathrm{Fe_3O_4}$$
$$\Delta G_r = \frac{1}{3}\Delta G_f(\mathrm{Fe_3O_4}) - \Delta G_f(\mathrm{FeO}) - \frac{1}{6}\Delta G_f(\mathrm{O_2}) \quad (9)$$

$$\frac{1}{3}\mathrm{Fe_3O_4} + \frac{1}{12}\mathrm{O_2} \rightleftarrows \frac{1}{2}\mathrm{Fe_2O_3}$$
$$\Delta G_r = \frac{1}{2}\Delta G_f(\mathrm{Fe_2O_3}) - \frac{1}{3}\Delta G_f(\mathrm{Fe_3O_4}) - \frac{1}{12}\Delta G_f(\mathrm{O_2}) \quad (10)$$

DOI: 10.1021/acs.jctc.6b00640
J. Chem. Theory Comput. 2016, 12, 5132−5144

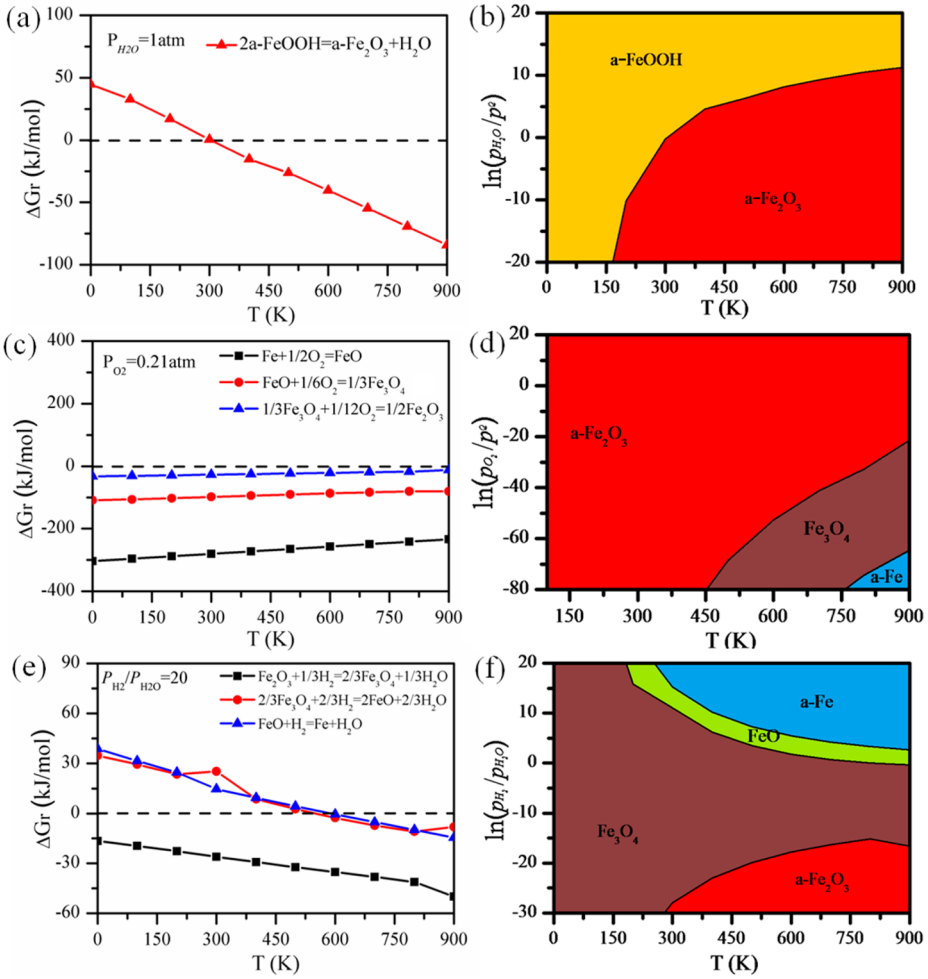

Figure 7. Thermodynamic equilibrium phase diagrams of iron oxides under different conditions: (a) relationship between the reaction free energy for dehydration of α-FeOOH to α-Fe_2O_3 and temperature at P_{H_2O} = 1 atm; (b) phase diagram for dehydration of α-FeOOH to α-Fe_2O_3; (c) relationships between the reaction free energies of the three oxidation reactions and temperature in standard atmosphere; (d) phase diagram of iron oxides under O_2 conditions; (e) relationships between the reaction free energies of the three reduction reaction and temperature at P_{H_2}/P_{H_2O} = 20; (f) phase diagram of iron oxides under H_2 reduction conditions.

$$\mathrm{Fe_2O_3} + \frac{1}{3}\mathrm{H_2} \rightleftarrows \frac{2}{3}\mathrm{Fe_3O_4} + \frac{1}{3}\mathrm{H_2O}$$

$$\Delta G_r = \frac{2}{3}\Delta G_f(\mathrm{Fe_3O_4}) + \frac{1}{3}\Delta G_f(\mathrm{H_2O}) - \Delta G_f(\mathrm{Fe_2O_3}) - \frac{1}{3}\Delta G_f(\mathrm{H_2}) \quad (11)$$

$$\frac{2}{3}\mathrm{Fe_3O_4} + \frac{2}{3}\mathrm{H_2} \rightleftarrows 2\mathrm{FeO} + \frac{2}{3}\mathrm{H_2O}$$

$$\Delta G_r = 2\Delta G_f(\mathrm{FeO}) + \frac{2}{3}\Delta G_f(\mathrm{H_2O}) - \frac{2}{3}\Delta G_f(\mathrm{Fe_3O_4}) - \frac{2}{3}\Delta G_f(\mathrm{H_2}) \quad (12)$$

$$\mathrm{FeO} + \mathrm{H_2} \rightleftarrows \mathrm{Fe} + \mathrm{H_2O}$$

$$\Delta G_r = \Delta G_f(\mathrm{Fe}) + \Delta G_f(\mathrm{H_2O}) - \Delta G_f(\mathrm{FeO}) - \Delta G_f(\mathrm{H_2}) \quad (13)$$

The reaction Gibbs free energies and equilibrium phase diagram for the three iron oxides under O_2 conditions are plotted in Figure 7c,d. Under air conditions, α-Fe_2O_3, rather than Fe_3O_4 or FeO, is the final state below 900 K because α-Fe_2O_3 is the most thermodynamically stable under these conditions. Figure 7d further indicates that each oxide has a characteristic region at a given temperature and pressure, and it reveals the difference in their thermodynamic stabilities. α-Fe_2O_3 is most favorable in the low-temperature region at a given O_2 pressure, and the region of α-Fe_2O_3 increases with increasing O_2 pressure at a given temperature. With increasing temperature, Fe_3O_4 and Fe become the most stable at low O_2 pressure in sequence. However, the FeO phase does not appear all the time, which indicates that FeO is not the most thermodynamically stable under O_2 conditions.

The reaction Gibbs free energies and equilibrium phase diagram for the three iron oxides under H_2 reduction conditions are shown in Figure 7e,f. Figure 7e presents the relationships between the reaction free energies of the three reduction reactions and the temperature at the given condition P_{H_2}/P_{H_2O} = 20. One can see that reduction of α-Fe_2O_3 to Fe_3O_4 is the thermodynamically spontaneous reaction at low temperature, while Fe_3O_4 reduction to FeO or Fe is unfavorable until the temperature goes up to 600 K. With increasing temperature, the equilibria of the three reduction reactions shift to the right.

DOI: 10.1021/acs.jctc.6b00640
J. Chem. Theory Comput. 2016, 12, 5132−5144

Figure 7f further presents the relationship between the most stable iron oxide phase and the temperature and P_{H_2}/P_{H_2O} ratio. α-Fe_2O_3 is not more favorable than Fe_3O_4 with temperature decreasing to a critical value at low P_{H_2}/P_{H_2O} ratios, while Fe_3O_4 continues to transform to FeO and finally to Fe metal with temperature increasing to a transition point at high P_{H_2}/P_{H_2O} conditions. Thus, each iron oxide has a region where it is the most stable under the temperature and pressure conditions. On the basis of this phase diagram, one can know the stable iron oxide at any given T and P_{H_2}/P_{H_2O} ratio.

4. CONCLUSIONS

We systematically investigated the ground-state properties of four iron oxides (α-FeOOH, α-Fe_2O_3, Fe_3O_4, and FeO) using different DFAs, namely, standard PBE, PBE+U with different values of U, and HSE with various percentages of HF exchange. We examined the lattice parameters, magnetism, electronic structures, and formation energies of the iron oxides using these three DFAs. We found that the HSE (a = 0.15) hybrid functional provides the most balanced and reliable results for a majority of the properties of the four iron oxides, while the PBE, PBE+U, and HSE (a = 0.25) methods have different deviations in predicting the magnetic, electronic and thermodynamic properties of the iron oxides, as argued below:

(1) PBE can provide good lattice parameters with a small error of 1% but significantly underestimates the Fe magnetic moments, formation energies, and band gaps of all four iron oxides by about 20−80%. What is worse is that PBE cannot predict reasonable electronic structures for all of the iron oxides.

(2) The PBE+U method is an effective corrected means to improve the electronic properties and band gap. The problem is that there is no single U value that can satisfactorily reproduce a majority of the properties for the four iron oxides. In order to make a meaningful comparison among the thermodynamic quantities of the iron oxides, it is unavoidable to make a compromise to choose a consistent U value. The suitable value of U for predicting acceptable band gaps and electronic structures of the four iron oxides varies from 3.6 to 5.0 eV. However, to obtain good formation energies, the suitable value of U is about 3 eV.

(3) For the HSE hybrid functional, the extensively used HSE (a = 0.25) functional seriously overestimates the band gaps and formation energies of iron oxides. The HSE (a = 0.15) functional presents good and balanced results for the structures, magnetism, electronic features, and formation energies for all of the iron oxides we studied. The calculations indicate that HSE (a = 0.10) underestimates the band gaps. Thus, HSE (a = 0.15) is a reliable choice for simulating the structures and major properties of the strongly related iron oxides.

In addition, we calculated the reaction Gibbs free energies of transformations among the iron oxides by DFT employing the HSE (a = 0.15) functional and plotted the thermodynamic phase diagrams of iron oxides under different conditions. The results are helpful to understand the most stable phase under given conditions, and one can optimize the conditions to synthesize the targeted iron oxide with this valuable information.

Here we have to point out that the final solutions on theory for strongly correlated systems are still on the way. To develop a highly efficient and parameter-free approach suitable to cope with complex transition metal−oxide systems is the goal. It is important to perform detailed benchmarks before such approaches will be used to solve practical problems and fundamental puzzles.

■ ASSOCIATED CONTENT

Supporting Information

The Supporting Information is available free of charge on the ACS Publications website at DOI: 10.1021/acs.jctc.6b00640.

Structural optimization E−V curves for the four iron oxides obtained using the PBE, PBE+U (4 eV), HSE (a = 0.25), and HSE (a = 0.15) methods; effect of the U value on the lattice parameters, Fe magnetic moments, and band gaps of the four iron oxides; TDOS of the four iron oxides calculated using PBE+U with U increasing from 0 to 6 (7) eV; calculated dielectric functions of the four iron oxides using PBE, PBE+U (4 eV), HSE (a = 0.25), and HSE (a = 0.15), including the real (Re) and imaginary (Im) parts; calculated phonon band structures, phonon TDOS, and Fe and O phonon partial densities of states obtained using HSE (a = 0.15); comparison of phonon DOS of α-Fe_2O_3 calculated using PBE, PBE+U (4 eV), and HSE (a = 0.15); convergence tests of total energy with decreasing k mesh size for HSE calculations; relative energies calculated using PBE, PBE+U (4 eV), HSE (a = 0.25), and HSE (a = 0.15) for four different magnetic ordering states (FM, AF, FiM, and NM); specific Fe magnetic moments (in μ_B) of differently coordinated Fe atoms in low-temperature Fe_3O_4; and Bader charge analyses of the four iron oxides by PBE, PBE+U (4 eV), HSE (a = 0.25), and HSE (a = 0.15) (PDF)

■ AUTHOR INFORMATION

Corresponding Authors

*E-mail: wxd@sxicc.ac.cn.

*E-mail: ywl@sxicc.ac.cn.

Funding

The authors are grateful for the financial support from the National Natural Science Foundation of China (21473229, 91545121, and 21273261) and Synfuels China, Co. Ltd. We also acknowledge the Innovation Foundation of the Institute of Coal Chemistry, Chinese Academy of Sciences, the National Thousand Young Talents Program of China, the Hundred-Talent Program of the Chinese Academy of Sciences, and the Shanxi Hundred-Talent Program. The computational resources for the project were supplied by Synfuels China, Co. Ltd.

Notes

The authors declare no competing financial interest.

■ ACKNOWLEDGMENTS

We are grateful to Prof. Roald Hoffmann (Cornell University) for critical comments and suggestions.

■ DEDICATION

This article is dedicated to Dr. Richard L. Martin on the occasion of his retirement from Los Alamos National Laboratory.

■ REFERENCES

(1) Cornell, R. M.; Schwertmann, U. *The Iron Oxides: Structure, Properties, Reactions, Occurrences and Uses*; Wiley-VCH: Weinheim, Germany, 2003.

DOI: 10.1021/acs.jctc.6b00640
J. Chem. Theory Comput. 2016, 12, 5132−5144

(2) Wu, C.; Yin, P.; Zhu, X.; Ouyang, C.; Xie, Y. Synthesis of hematite (alpha-Fe_2O_3) nanorods: diameter-size and shape effects on their applications in magnetism, lithium ion battery, and gas sensors. *J. Phys. Chem. B* **2006**, *110*, 17806−17812.
(3) Zeng, S.; Tang, K.; Li, T.; Liang, Z.; Wang, D.; Wang, Y.; Zhou, W. Hematite Hollow Spindles and Microspheres: Selective Synthesis, Growth Mechanisms, and Application in Lithium Ion Battery and Water Treatment. *J. Phys. Chem. C* **2007**, *111*, 10217−10225.
(4) Li, P.; Miser, D. E.; Rabiei, S.; Yadav, R. T.; Hajaligol, M. R. The removal of carbon monoxide by iron oxide nanoparticles. *Appl. Catal., B* **2003**, *43*, 151−162.
(5) Mallinson, J. C. *The Foundations of Magnetic Recording*, 2nd ed.; Academic Press: New York, 1993.
(6) Geus, W. J. Preparation and properties of iron oxide and metallic iron catalysts. *Appl. Catal.* **1986**, *25* (1-2), 313−333.
(7) Liger, E.; Charlet, L.; Van Cappellen, P. Surface catalysis of uranium(VI) reduction by iron(II). *Geochim. Cosmochim. Acta* **1999**, *63*, 2939−2955.
(8) Herrera, F.; Lopez, A.; Mascolo, G.; Albers, P.; Kiwi, J. Catalytic combustion of Orange II on hematite: Surface species responsible for the dye degradation. *Appl. Catal., B* **2001**, *29*, 147−162.
(9) Huang, H. H.; Lu, M. C.; Chen, J. N. Catalytic decomposition of hydrogen peroxide and 2-chlorophenol with iron oxides. *Water Res.* **2001**, *35*, 2291−2299.
(10) Ning, W. S.; Koizumi, N.; Chang, H.; Mochizuki, T.; Itoh, T.; Yamada, M. Phase transformation of unpromoted and promoted Fe catalysts and the formation of carbonaceous compounds during Fischer−Tropsch synthesis reaction. *Appl. Catal., A* **2006**, *312*, 35−44.
(11) Jin, Y. M.; Datye, A. K. Phase Transformations in Iron Fischer−Tropsch Catalysts during Temperature-Programmed Reduction. *J. Catal.* **2000**, *196*, 8−17.
(12) Marsman, M.; Paier, J.; Stroppa, A.; Kresse, G. Hybrid functionals applied to extended systems. *J. Phys.: Condens. Matter* **2008**, *20*, 064201−064210.
(13) Tran, F.; Blaha, P.; Schwarz, K.; Novak, P. Hybrid exchange-correlation energy functionals for strongly correlated electrons: Applications to transition-metal monoxides. *Phys. Rev. B: Condens. Matter Mater. Phys.* **2006**, *74*, 155108.
(14) Rivero, P.; Moreira, I. P. R.; Scuseria, G. E.; Illas, F. Description of magnetic interactions in strongly correlated solids via range-separated hybrid functional. *Phys. Rev. B: Condens. Matter Mater. Phys.* **2009**, *79*, 245129.
(15) Anisimov, V. I.; Zaanen, J.; Andersen, O. K. Band theory and Mott insulators: Hubbard U instead of Stoner. *Phys. Rev. B: Condens. Matter Mater. Phys.* **1991**, *44*, 943.
(16) Becke, A. D. A new mixing of Hartree−Fock and local density functional theories. *J. Chem. Phys.* **1993**, *98*, 1372.
(17) Perdew, J.; Ernzerhof, M.; Burke, K. Rationale for mixing exact exchange with density functional approximations. *J. Chem. Phys.* **1996**, *105*, 9982.
(18) Kubicki, J. D.; Paul, K. W.; Sparks, D. L. Periodic density functional theory calculations of bulk and the (010) surface of goethite. *Geochem. Trans.* **2008**, *9*, 4−19.
(19) Rosso, K. M.; Rustad, J. R. Structures and energies of AlOOH and FeOOH polymorphs from plane wave pseudopotential calculation. *Am. Mineral.* **2001**, *86*, 312−317.
(20) Tunega, D. Theoretical Study of Properties of Goethite (α-FeOOH) at Ambient and High-Pressure Conditions. *J. Phys. Chem. C* **2012**, *116*, 6703−6713.
(21) Liao, P. L.; Carter, E. A. Testing variations of the GW approximation on strongly correlated transition metal oxides: hematite (α-Fe_2O_3) as a benchmark. *Phys. Chem. Chem. Phys.* **2011**, *13*, 15189−15199.
(22) Rowan, A. D.; Patterson, C. H.; Gasparov, L. V. Hybrid density functional theory applied to magnetite: Crystal structure, charge order, and phonons. *Phys. Rev. B: Condens. Matter Mater. Phys.* **2009**, *79*, 205103.
(23) Alfredsson, M.; Price, G. D.; Catlow, C. R. A.; Parker, S. C.; Orlando, R.; Brodholt, J. P. Electronic structure of the antiferromagnetic B1-structured FeO. *Phys. Rev. B: Condens. Matter Mater. Phys.* **2004**, *70*, 165111.
(24) Rollmann, G.; Rohrbach, A.; Entel, P.; Hafner, J. First-principles calculation of the structure and magnetic phases of hematite. *Phys. Rev. B: Condens. Matter Mater. Phys.* **2004**, *69*, 165107.
(25) Pozun, Z. D.; Henkelman, G. Hybrid density functional theory band structure engineering in hematite. *J. Chem. Phys.* **2011**, *134*, 224706.
(26) Wilson, N. C.; Russo, S. P. Hybrid density functional theory study of the high pressure polymorphs of α-Fe_2O_3 hematite. *Phys. Rev. B: Condens. Matter Mater. Phys.* **2009**, *79*, 094113.
(27) Toroker, M. C.; Kanan, D. K.; Alidoust, N.; Isseroff, L. Y.; Liao, P.; Carter, E. A. First principles scheme to evaluate band edge positions in potential transition metal oxide photocatalysts and photoelectrodes. *Phys. Chem. Chem. Phys.* **2011**, *13*, 16644−16654.
(28) Jeng, H. T.; Guo, G. Y.; Huang, D. J. Charge-Orbital Ordering and Verwey Transition in Magnetite. *Phys. Rev. Lett.* **2004**, *93*, 156403.
(29) Leonov, I.; Yaresko, A. N.; Antonov, V. N.; Korotin, M. A.; Anisimov, V. I. Charge and Orbital Order in Fe_3O_4. *Phys. Rev. Lett.* **2004**, *93*, 146404.
(30) Liao, P. L.; Carter, E. A. Ab initio DFT + U predictions of tensile properties of iron oxides. *J. Mater. Chem.* **2010**, *20*, 6703−6719.
(31) Zhang, W. B.; Deng, Y. H.; Hu, Y.-L.; Han, K.-L.; Tang, B. Y. Structural distortion of B1-structured MnO and FeO. *Solid State Commun.* **2007**, *142*, 6−9.
(32) Heyd, J.; Scuseria, G. E.; Ernzerhof, M. Hybrid functionals based on a screened Coulomb potential. *J. Chem. Phys.* **2003**, *118*, 8207−8215.
(33) Heyd, J.; Scuseria, G. E. Efficient hybrid density functional calculations in solids: Assessment of the Heyd−Scuseria−Ernzerhof screened Coulomb hybrid functional. *J. Chem. Phys.* **2004**, *121*, 1187−1192.
(34) Feng, X.; Harrison, N. M. Magnetic coupling constants from a hybrid density functional with 35% Hartree-Fock exchange. *Phys. Rev. B: Condens. Matter Mater. Phys.* **2004**, *70*, 092402.
(35) Ciofini, I.; Illas, F.; Adamo, C. Performance of the tau-dependent functionals in predicting the magnetic coupling of ionic antiferromagnetic insulators. *J. Chem. Phys.* **2004**, *120*, 3811−3816.
(36) Wen, X. D.; Martin, R. L.; Henderson, T. M.; Scuseria, G. E. Density Functional Theory Studies of the Electronic Structure of Solid State Actinide Oxides. *Chem. Rev.* **2013**, *113*, 1063−1096.
(37) Russell, B.; Payne, M.; Ciacchi, L. C. Density functional theory study of Fe(II) adsorption and oxidation on goethite surfaces. *Phys. Rev. B: Condens. Matter Mater. Phys.* **2009**, *79*, 165101.
(38) Otte, K.; Pentcheva, R.; Schmahl, W. W.; Rustad, J. R. Pressure-induced structural and electronic transitions in FeOOH from first principles. *Phys. Rev. B: Condens. Matter Mater. Phys.* **2009**, *80*, 205116.
(39) Lemaire, B. J.; Davidson, P.; Ferré, J.; Jamet, J. P.; Panine, P.; Dozov, I.; Jolivet, J. P. Outstanding Magnetic Properties of Nematic Suspensions of Goethite (α-FeOOH) Nanorods. *Phys. Rev. Lett.* **2002**, *88*, 125507.
(40) Cox, D. E.; Takei, W. J.; Miller, R. C.; Shirane, G. A magnetic and neutron diffraction study of the Fe_2O_3-V_2O_3 system. *J. Phys. Chem. Solids* **1962**, *23*, 863−874.
(41) Kren, E.; Szabo, P.; Konczos, G. Neutron diffraction studies on the (1−x)Fe_2O_3-xRh_2O_3 system. *Phys. Lett.* **1965**, *19* (2), 103−104.
(42) Coey, J. M. D.; Sawatzky, G. A. A study of hyperfine interactions in the system $(Fe_{1-x}Rh_x)_2O_3$ using the Mossbauer effect (Bonding parameters). *J. Phys. C: Solid State Phys.* **1971**, *4*, 2386.
(43) Finger, L. W.; Hazen, R. M. Crystal structure and isothermal compression of Fe_2O_3, Cr_2O_3, and V_2O_3 to 50 Kbars. *J. Appl. Phys.* **1980**, *51*, 5362−5367.
(44) Szotek, Z.; Temmerman, Z. S.; Svane, A.; Petit, L.; Stocks, G. M.; Winter, H. Ab initio study of charge order in Fe_3O_4. *Phys. Rev. B: Condens. Matter Mater. Phys.* **2003**, *68*, 054415.
(45) Wright, J. P.; Attfield, J. P.; Radaelli, P. G. Long Range Charge Ordering in Magnetite Below the Verwey Transition. *Phys. Rev. Lett.* **2001**, *87*, 266401; Charge ordered structure of magnetite Fe_3O_4 below the Verwey transition. *Phys. Rev. B: Condens. Matter Mater. Phys.* **2002**, *66*, 214422.

DOI: 10.1021/acs.jctc.6b00640
J. Chem. Theory Comput. 2016, 12, 5132−5144

(46) Huang, D. J.; Chang, C. F.; Jeng, H. T.; Guo, G. Y.; Lin, H.-J.; Wu, W. B.; Ku, H. C.; Fujimori, A.; Takahashi, Y.; Chen, C. T. Spin and Orbital Magnetic Moments of Fe_3O_4. *Phys. Rev. Lett.* **2004**, *93*, 077204.
(47) Park, S. K.; Ishikawa, T.; Tokura, Y. Charge-gap formation upon the Verwey transition in Fe_3O_4. *Phys. Rev. B: Condens. Matter Mater. Phys.* **1998**, *58*, 3717.
(48) Rodl, C.; Fuchs, F.; Furthmuller, J.; Bechstedt, F. Quasiparticle band structures of the antiferromagnetic transition-metal oxides MnO, FeO, CoO, and NiO. *Phys. Rev. B: Condens. Matter Mater. Phys.* **2009**, *79*, 235114.
(49) Gorton, A. T.; Bitsianes, G.; Joseph, T. L. Thermal Expansion Coefficients for Iron and its Oxides From X-Ray Diffraction Measurements At Elevated Temperatures. *Trans. Metall. Soc. AIME* **1965**, *233*, 1519−1525.
(50) Roth, W. L. Magnetic structures of MnO, FeO, CoO, and NiO. *Phys. Rev.* **1958**, *110*, 1333.
(51) Battle, P. D.; Cheetham, A. K. The magnetic structure of non-stoichiometric ferrous oxide. *J. Phys. C: Solid State Phys.* **1979**, *12*, 337.
(52) Blöchl, P. E. Projector augmented-wave method. *Phys. Rev. B: Condens. Matter Mater. Phys.* **1994**, *50*, 17953.
(53) Kresse, G.; Hafner, J. Ab initio molecular dynamics for liquid metals. *Phys. Rev. B: Condens. Matter Mater. Phys.* **1993**, *47*, 558.
(54) Perdew, J. P.; Burke, K.; Ernzerhof, M. Generalized Gradient Approximation Made Simple. *Phys. Rev. Lett.* **1996**, *77*, 3865.
(55) Dudarev, S. L.; Botton, G. A.; Savrasov, S. Y.; Humphreys, C. J.; Sutton, A. P. Electron-energy-loss spectra and the structural stability of nickel oxide: An LSDA+*U* study. *Phys. Rev. B: Condens. Matter Mater. Phys.* **1998**, *57*, 1505.
(56) Krukau, A. V.; Vydrov, O. A.; Izmaylov, A. F.; Scuseria, G. E. Influence of the exchange screening parameter on the performance of screened hybrid functional. *J. Chem. Phys.* **2006**, *125*, 224106.
(57) Noh, J.; Osman, I. O.; Aziz, S. G.; Winget, P.; Brédas, J. L. A density functional theory investigation of the electronic structure and spin moments of Magnetite. *Sci. Technol. Adv. Mater.* **2014**, *15*, 044202.
(58) Chuang, Y.-Y.; Schmid, R.; Chang, Y. A. Magnetic contributions to the thermodynamic functions of pure Ni, Co, and Fe. *Metall. Trans. A* **1985**, *16*, 153−165.
(59) Togo, A.; Oba, F.; Tanaka, I. First-principles calculations of the ferroelastic transition between rutile-type and CaCl2-type SiO2 at high pressures. *Phys. Rev. B: Condens. Matter Mater. Phys.* **2008**, *78*, 134106.
(60) Nagai, T.; Kagi, H.; Yamanaka, T. Variation of hydrogen bonded O-O distances in goethite at high pressure. *Am. Mineral.* **2003**, *88*, 1423−1427.
(61) Merchant, P.; Collins, R.; Kershaw, R.; Dwight, K.; Wold, A. The electrical, optical and photoconducting properties of $Fe_{2-x}Cr_xO_3$ ($0 < x < 0.47$). *J. Solid State Chem.* **1979**, *27* (3), 307−315.
(62) Haavik, C.; Stolen, S.; Fjellvag, H.; Hanfland, M.; Hausermann, D. Equation of state of magnetite and its high-pressure modification: Thermodynamics of the Fe-O system at high pressure. *Am. Mineral.* **2000**, *85*, 514−523.
(63) Bowen, H. K.; Adler, D.; Auker, B. H. Electrical and optical properties of FeO. *J. Solid State Chem.* **1975**, *12*, 355.
(64) Hazen, R. M.; Finger, L. W. Bulk moduli and high-pressure crystal structures of rutile-type compounds. *J. Phys. Chem. Solids* **1981**, *42*, 143−151.
(65) Zimmermann, R.; Steiner, P.; Claessen, R.; Reinert, F.; Hüfner, S.; Blaha, P.; Dufek, P. Electronic structure of 3d-transition-metal oxides: on-site Coulomb repulsion versus covalency. *J. Phys.: Condens. Matter* **1999**, *11*, 1657−1682.
(66) Stull, D. R.; Prophet, H. *JANAF Thermochemical Tables*, 2nd ed.; U.S. National Bureau of Standards: Washington, DC, 1971.

DOI: 10.1021/acs.jctc.6b00640
J. Chem. Theory Comput. 2016, 12, 5132−5144